Austrian Marshall Plan Scholarship Research Paper

The dynamic assembly and disassembly of the ESCRT machinery

Mehrshad Pakdel
mehrshad.pakdel@gmail.com
December 2014

Supervisors:

Assoc. Prof. Dr. rer. nat. David Teis
Biocenter, Innsbruck Medical University
Innsbruck, Austria

Prof. Tomas Kirchhausen, Ph.D.
Harvard Medical School / Program in Cellular and Molecular Medicine
Boston (MA), U.S.A.

Contents

1 Acknowledgements

First and foremost I am grateful to my supervisor David Teis who gave me the opportunity to work in his lab and included me early on in important projects. His dedication to science was encouraging every day. He supported me not only during my Master's Thesis but also during the Marshall Plan Scholarships application and during my stay in Boston.

I would like to express my gratitude to Tomas Kirchhausen who supported our research proposal of the ESCRT imaging project from the beginning on and invited me to his lab to Harvard Medical School / Program in Cellular and Molecular Medicine in Boston (MA). It was an amazing experience to be a part of his lab and getting insights to advanced fluorescence microscopy techniques.

Besides my advisors, I would like to thank Mithun Pasham for introducing me to the lab and teaching me to operate the Spinning Disc Confocal microscope. Thanks to Srigokul Upadhyayula for generation of Matlab scripts and all the questions concerning the computational analysis.

I would like to thank Manuel Alonso Y Adell and Simona Migliano for generating missing strains and plasmids and for sending me all these FedEx folders.

I am grateful to the Austrian Marshall Plan Foundation (Walcherstraße 11A, 1020 Wien, Austria), which made this experience possible through their financial support.

Beyond science, I want to thank my parents and my girlfriend Alina for their caring support and encouragement throughout the time in Boston.

2 Abstract

The multivesicular body (MVB) pathway is required for the delivery and the degradation of ubiquitinated integral membrane proteins (cargo) into lysosomes. On endosomes, five endosomal sorting complexes required for transport (ESCRT) mediate recognition of ubiquitinated cargo, cargo sorting and intraluminal vesicle (ILV) formation. ESCRT-0, -I, -II bind directly to ubiquitinated membrane proteins and ESCRT-III together with the AAA-ATPase Vps4 is required to drive membrane invagination and scission. Thereby, Vps4 disassembles the ESCRT-III complex and terminates the ESCRT pathway. The dynamic properties of the ESCRT-machinery are not understood. By investigating fluorescently tagged functional Vps4 through live-cell Spinning Disc Confocal microscopy and single molecule imaging, we found that Vps4 localizes to endocytic vesicles and shows dynamic assembly and disassembly events whereas the ATPase deficient mutant Vps4-E233Q shows no such events rather decays in its intensity over time. Additionally, we could reveal that Vps4 appears as a monomer/dimer equilibrium in the cytosol and can oligomerize to the smallest unit of a hexameric complex. The majorities of vesicles show 6 - 36 molecules of Vps4, but rarely are associated with more. Conclusively, we could set up an acquisition system for baker's yeast in order to identify the oligomeric state of Vps4 in the cytoplasm, its dynamic properties over time and its preferential complex distribution. In this way, we contributed with this project for the first time to the understanding of dynamics of the ESCRT machinery during ILV biogenesis *in vivo*.

3 Introduction

The degradation of integral membrane proteins in lysosomes via the multivesicular body (MVB) pathway is essential for the regulation of cell surface signaling during cell homeostasis and development (Schmidt and Teis, 2012).

The MVB pathway is particularly crucial for the selective removal and the degradation of signaling growth factor receptors (e.g. the epidermal growth factor receptor, EGFR). Once activated by their cognate ligands (e.g. EGF) receptors not only trigger intracellular signaling cascades but also become selectively ubiquitinated (Huang et al., 2006). Ubiquitinated receptors like EGFR, transferrin receptor (TfR) and low-density lipoprotein receptor (LDLR) are selectively removed from the cell surface by clathrin mediated endocytosis (Kirchhausen et al., 2014). The heterotetrameric adaptor complex AP2 while also associating with clathrin recognizes signal sequences within the cytoplasmic tails of these receptors. As clathrin assembles into a coat on the plasma membrane, it forms a pit harboring multiple species of cargos and it begins to pull the membrane into the cell (Kirchhausen et al., 2014). The GTPase Dynamin is recruited as dimers at the constricted neck of clathrin coated pits and assembled into helical polymers around the constricted neck (Cocucci et al., 2014; Ferguson and De Camilli, 2012). Finally, upon GTP hydrolysis Dynamin executes the scission of the neck that connects the growing clathrin coated vesicle with the plasma membrane (Cocucci et al., 2014; Ferguson and De Camilli, 2012). In this way cargo such as epidermal growth factor receptor (EGFR), which initiates strong downstream proliferation signals upon ligand binding, are removed from the cell surface and delivered to endosomes (Bache, 2006). On endosomes ubiquitinated membrane proteins are then sorted via the MVB pathway into lysosomes where they are ultimately degraded by acidic hydrolases (Henne et al., 2011).

The Endosomal Sorting Complexes Required for Transport (ESCRT) are key mediators of the MVB pathway (Figure 1. Adapted from Teis et al., 2009). The core of the evolutionary conserved ESCRT-machinery consists of 14 different genes that assembly into five distinct evolutionary highly conserved protein complexes ESCRT-0, -I, -II, -III and Vps4 (Teis et al., 2009). Their sequential recruitment to endosomes is essential for ubiquitinated cargo recognition and sorting, intraluminal vesicle (ILV) budding and abscission towards the lumen of endosomes (Henne et al., 2012; Schmidt and Teis, 2012).

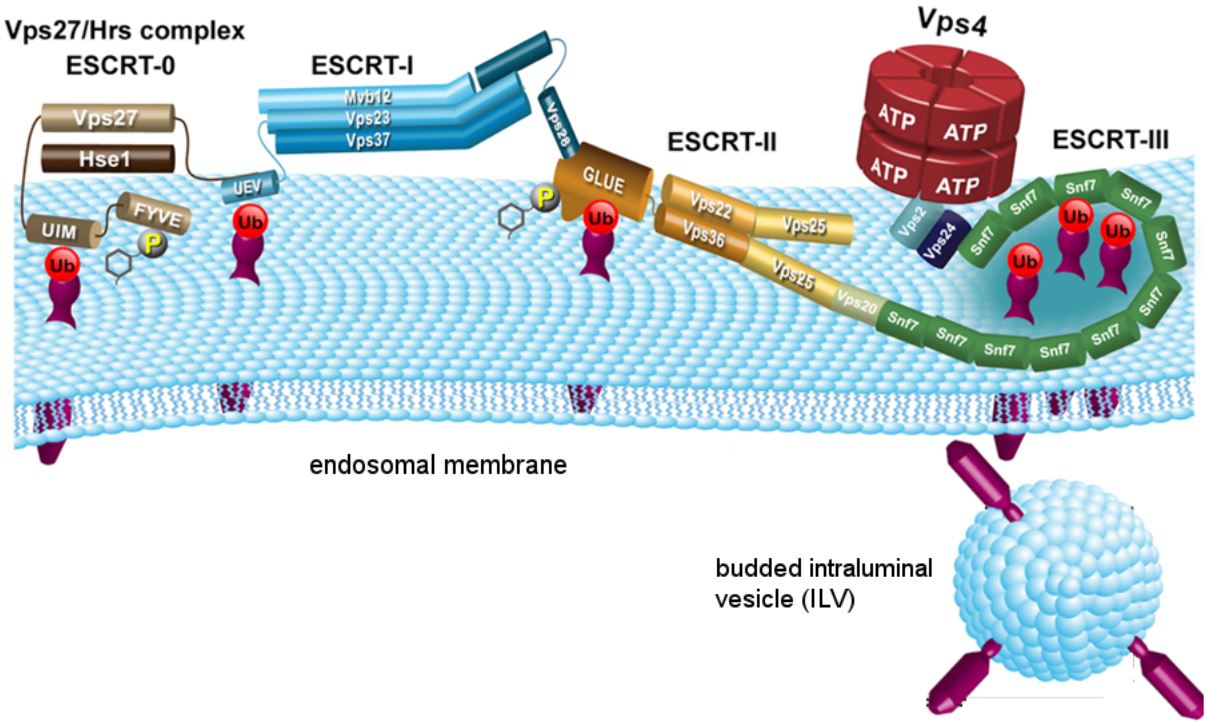

Figure 1. Schematic overview of the ESCRT-0, -I, -II, -III and Vps4. Ubiquitinated membrane proteins destined for degradation are recognized and sorted by early ESCRT-0, -I and –II. ESCRT-II then recruits ESCRT-III and nucleates ESCRT-III to a ring like filament. Upon assembly of ESCRT-III, Vps4 binds to ESCRT-III and disassembles the complex. During this step cargo laden intraluminal vesicles are formed and bud into the endosomal lumen (adapted from Teis et al., 2009).

The basics of the assembly of the ESCRT machinery are known: ESCRT-0 is a heterodimer consisting of Vps27 and Hse1. The FYVE domain of Hrs binds to phosphatidylinositol 3-phosphate (PI3P), a specific phospholipid that is enriched on endosomes. This provides the specific recruitment of ESCRT-0 to endosomal membranes (Henne et al., 2011). Both subunits also interact with ubiquitinated membrane proteins to target cargo-enriched endosomes and for cargo sorting (Henne et al., 2011). ESCRT-0 then recruits ESCRT-I which is a hetero-tetrameric complex consisting of Vps23, Vps28, Vps37 and the associated non-essential subunit Mvb12 (Henne et al., 2011). On endosomes, ESCRT-I binds also to ubiquitinated membrane proteins and interacts with the ESCRT-II complex. ESCRT-II consists of Vps36, Vps22 and Vps25. ESCRT-II is a central player that binds to PI3P, ubiquitinated membrane proteins and also scaffold the assembly of the ESCRT-III complex (Figure 1) (Teis et al., 2010).

In contrast to ESCRT-0,-I,-II which are recruited as preassembled complexes from the cytoplasm to the surface of endosomes, the ESCRT-III complex only assembles on endosomes (Babst et al., 2002a, 2002b).

The ESCRT-II component Vps25 recruits the first ESCRT-III subunit Vps20 which then nucleates oligomers of ESCRT-III subunit Snf7 to a ring like filament structure (Figure 1) (Henne et al., 2012; Teis et al., 2010). This homo-oligomerization of Snf7 is capped by the recruitment of Vps24 which then recruits the last ESCRT-III subunit Vps2 to the complex (Figure 1) (Teis et al., 2008). Once ESCRT-III assembly is complete, Vps2 recruits the AAA-ATPase Vps4, which assembles into a functional homo-hexameric or dodecameric enzyme and binds ESCRT-III (Babst, 1998; Monroe et al., 2014). This homo-oligomerization was reported to be ATP dependent and is stabilized by the co-factor Vta1 (Xiao et al., 2008). Vta1 dimerizes with its C-terminal domain and forms a complex with Vps4 promoting its ATPase activity, thus acting as a positive regulator of Vps4 (Azmi, 2006; Xiao et al., 2008).

Vps4 interacts with the ESCRT-III complex via its N-terminus, the so called MIT (microtubule interacting and transport) domain which binds to the MIM (MIT-interacting motif) of Snf7 and Vps2 (Adell et al., 2014). Point mutations within the MIM domains of Snf7 and Vps2 (*snf7*-L199D and *vps2*-L228D, K229D), efficiently inhibit the binding of Vps4 to ESCRT-III whereas point mutation within the MIM domains of Vps20 (*vps20*-L188D) and Vps24 (*vps24*-R218D) did not affect binding of Vps4 to ESCRT-III subunits (Adell et al., 2014). Interestingly, by combining Snf7 and Vps2 MIM mutations in double mutants, the binding of Vps4 to ESCRT-III is synergistically decreased, suggesting that Vps2 and Snf7 play a major role in Vps4 recruitment and binding (Adell et al., 2014). Upon ATP hydrolysis Vps4 disassembles the whole ESCRT-III complex thus releases ESCRT-III subunits into the cytoplasm. This is achieved by the coordinated binding of Vps4 to the ESCRT-III complex which is directly coupled to membrane neck constriction during ILV biogenesis (Adell et al., 2014). In particular binding of Vps4 to Vps2 and Snf7 coordinates the disassembly of ESCRT-III subunits and membrane neck constriction (Adell et al., 2014). ESCRT-III subunits are then recycled into the cytoplasm and are not consumed during this reaction, enabling a new cycle of reassembly to endosomal membranes (Babst, 1998; Wollert and Hurley, 2010).

At the end of the reaction the ESCRT machinery has loaded ubiquitinated membrane proteins into ILV and has generated one ILV with a defined diameter of 25 nm. If

only one step in this complex machinery fails, membrane proteins are no longer degraded but instead accumulate in cells, which has deleterious consequences.

Recent studies have shown that disruption of ESCRT-I or –II or Vps4 leads to accumulation of receptors on endosomes, loss of cell polarity and epithelial integrity, and increased cell death (Rodahl et al., 2009). These properties are often associated with cancer development. In fact, abrogation of JNK signaling in Vps4 deficient cells prevents cell death and leads ultimately to the formation of tumors in the fruit fly *Drosophila melanogaster* (Rodahl et al., 2009). Furthermore, ESCRT function is required for the budding of several retroviruses including the human immunodeficiency virus (HIV). HIV highjacks ESCRT subunits during budding from the cell surface of infected host cells and catalyzes the scission of the membrane stalk that connects the budding virus with the host cell (Bleck et al., 2014; Carlton and Martin-Serrano, 2007). The membrane topology of this budding reaction corresponds to ILV biogenesis. Thus the ESCRT machinery buds membranes away from the cytoplasm, which is the opposite topology of membrane budding executed by Clathrin and other conventional coats.

Probably all core components of the ESCRT machinery have been identified, yet there are many open questions regarding the mechanism of the ESCRT machinery.

The goal of this study is to get a better understanding of the dynamic properties of the ESCRT machinery. So far it is clear that Vps4 efficiently disassembles the ESCRT-III complex *in vitro* and *in vivo* (Adell et al., 2014; Davies et al., 2010). However, how fast the actual reaction occurs and how it is executed is not understood so far.

Finally, the dynamics of the ESCRT subunits and ILV formation are still unknown. To get a better understanding about ESCRT dynamics we want to identify the lifetime of ESCRT complexes on endosomes and to quantify ESCRT subunits by single molecule imaging. Additionally, we want to focus on Vps4 and assess its oligomeric state in the cytosol and within a complex.

To address these questions we started a new collaboration with Tomas Kirchhausen (Program in Cellular and Molecular Medicine at Boston Children's Hospital, Harvard Medical School, Boston, MA) supported by the Austrian Marshall Plan Foundation to assess 'the dynamics of the ESCRT machinery' by investigating fully functional fluorescently tagged ESCRT-I, ESCRT-II and Vps4 subunits by Spinning Disc confocal microscopy with high temporal resolution and single molecule imaging.

4 Results

4.1 Generation of functional fluorescently tagged ESCRT subunits

As previously published, localization experiments with fluorescently tagged ESCRT subunits revealed the ordered assembly of the ESCRT-III complex (Teis et al., 2008). In particular, the correct localization of downstream ESCRT subunits to endosomal compartments was dependent of its upstream recruitment factors (Teis et al., 2008). These studies contributed to the understanding of the subsequent assembly and architecture of the ESCRT-III complex. So far, all fluorescently tagged ESCRT-III subunits were not functional as they were not able to promote cargo sorting resulting in accumulation of class-E compartments (Teis et al., 2008).

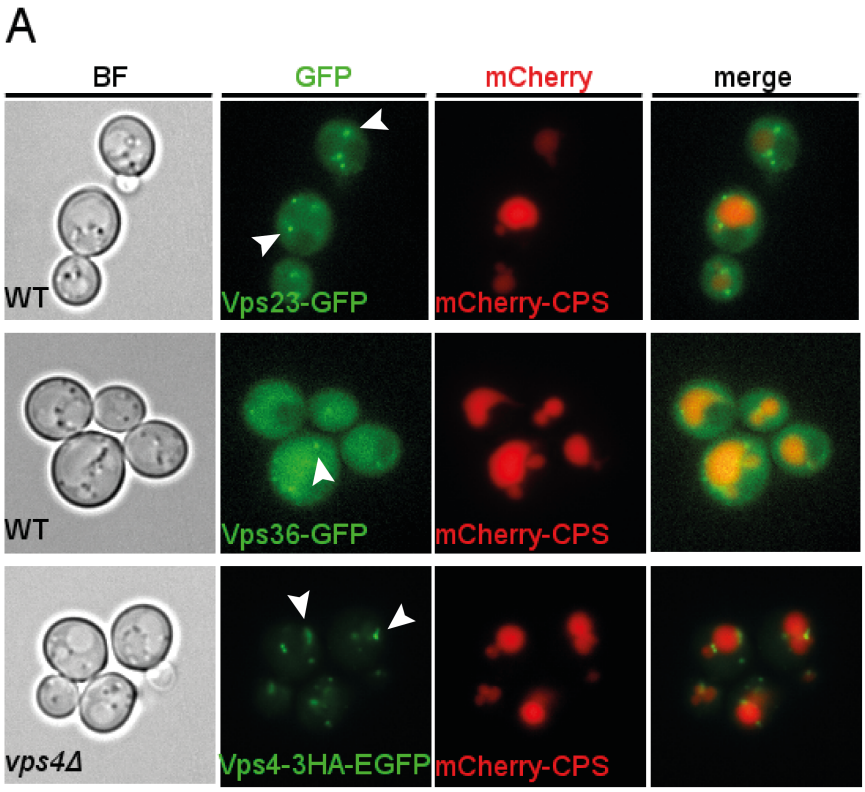

Figure 2A. Epifluorescence microscopy of fluorescently tagged ESCRT subunits. Left row: brightfield, green channel: GFP/EGFP, red channel: mCherry-CPS, right row: merge of GFP/EGFP and mCherry-CPS. Upper panel shows Vps23-GFP acquired with 1s exposure of one plane showing cytoplasmic signal and visible dots (white arrowheads). Middle panel shows Vps36-GFP (exp. 1s, one plane) with cytoplasmic signal and visible dots (white arrowheads). Lower panel shows *vps4Δ* complemented with Vps4-3HA-EGFP (exp. 0.3s, one plane) under an endogenous promotor. Vps4-3HA-EGFP shows stronger signals associated on dots (white arrowheads) relative to its cytoplasmic signal. mCherry-CPS is transported in all three cell lines to the lumen oft the vacuole.

Since we want to study the dynamics of this machinery in real time and *in vivo*, it is crucial to use functional fluorescently tagged subunits. Here, we generated functional Vps23-GFP (ESCRT-I), Vps36-GFP (ESCRT-II) (Figure 2A). Vps4-3HA-EGFP was expressed under an endogenous promoter in *vps4Δ* knockout cells (Figure 2A) or was introduced via chromosomal integration (data not shown). In this way, endogenous proteins are replaced with their respective EGFP-tagged version. Not only the localization to endosomes remains intact, but also the fluorescent-tagged subunits fulfill their proper function in ubiquitinated cargo sorting, recruitment of subsequent downstream ESCRT subunits, membrane scission and ESCRT-III subunit recycling. To demonstrate the functionality of these subunits, we transformed Vps23-GFP, Vps36-GFP and *vps4Δ*+Vps4-3HA-EGFP cells with the model cargo protein mCherry-CPS which is transported through the MVB pathway to the lumen of the vacuole indicating proper cargo sorting and a functional MVB pathway. Epifluorescence imaging reveals cytoplasmic Vps23-GFP signal as well as Vps23-GFP associated on dots, presumably endosomes (Figure2A, upper panel, white arrowheads). Similarly, Vps36-GFP shows cytoplasmic signal with some weak dots. (Figure 2A, middle panel, white arrowheads).

By contrast, *vps4Δ* cells complemented with Vps4-3HA-EGFP show higher signals on dots as in the cytoplasm (Figure 2A, lower panel, white arrowheads). Vps4 is the final factor that is recruited to endosomes and its recruitment is dependent on assembly of all ESCRT complexes (Migliano, Adell et. al., unpublished data). Contrary to this finding, subcellular fractionation experiments suggest the majority of Vps4 being in the cytoplasm rather than a minor fraction being associated with the membrane fraction which could be an indication for very fast subunit exchange (Adell et al., 2014). The explanation for this finding lies in the oligomerization of Vps4 to a hexameric or dodecameric ring increasing the fluorescence signal while more molecules assemble on endosomes whereas Vps36 does not oligomerize rather than assembles as a single molecule into the ESCRT-II complex (Im et al., 2009). The lower molecule numbers within a complex results in weaker endosomal signals. Due to higher copy numbers Vps4-3HA-EGFP was better to visualize and has a crucial role to terminate the ESCRT pathway. Thus, we decided to focus on Vps4-3HA-EGFP and therefore generated a chromosomal integrated version of Vps4-3HA-EGFP for all subsequent experiments.

4.2 Single Molecule Calibration

In this work we aim to assess the dynamics of Vps4-3HA-EGFP *in vivo* with advanced fluorescence microscopy in particular by using Spinning Disc Confocal microscopy with high spatial and temporal resolution.

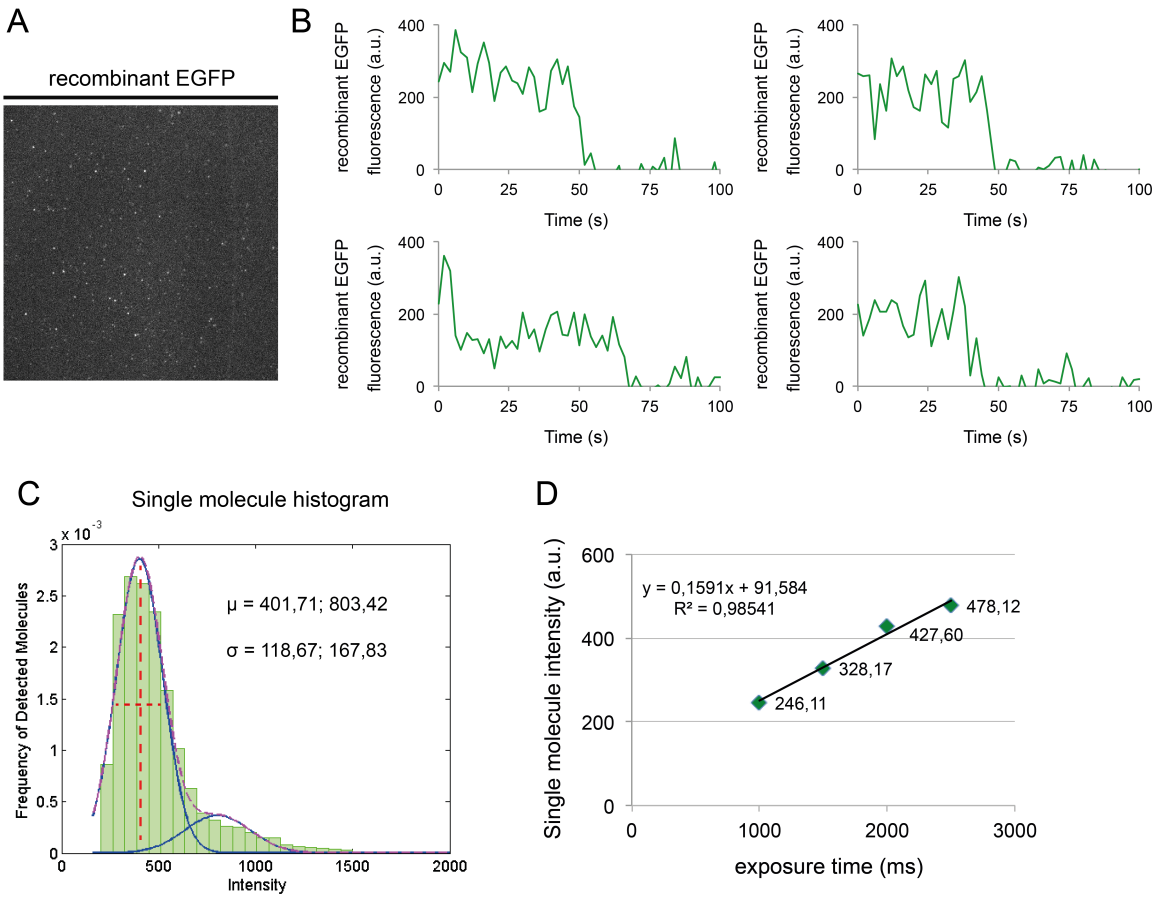

Figure 3. Single molecule calibration procedure by Spinning Disc Confocal microscopy. A: recombinant EGFP immobilizied on glass cover slips were acquired with an exposure of 2s for at least 50 consecutive frames. B: representative single-bleaching step graphs show the fluorophores bleaching pattern over time of one molecule of EGFP, respectively. C: the amplitudes of these steps of at least three different field of views were combined into a histogram plot showing two populations of EGFP molecules (green) and fitted with a Gaussian function (blue lines, mangenta line). The vertical dashed red line indicates the mean (μ) of 401,71 fluorescence intensites and the horizontal dashed red line represents the variance (σ) 118,67 fluorescence intensities of the first molecule population. D: the graph shows the plot of the mean intensities of single molecule histograms acquired with increasing exposure times ranging from 1 – 2.5s.

To determine how many molecules of Vps4 are involved in ESCRT-III recycling and membrane scission during MVB biogenesis, we performed single molecule imaging as previously described (Cocucci et al., 2012; Kural et al., 2012). Calculating molecule numbers from fluorescence intensities requires single molecule calibration of the microscope in advance to Vps4-3HA-EGFP cell samples. Recombinant EGFP purified from *E.Coli* was immobilized on glass cover slips and detected by Spinning Disc Confocal microscopy by acquiring at least 50 consecutive frames with exposure times ranging from 1s – 2.5s (Figure 3A). Subsequent computational analysis with custom-made Matlab scripts detect diffraction limited spots, their amplitudes and thus obtaining single-bleaching steps of single molecules (Figure 3B). The amplitudes of these steps were plotted as a histogram showing the Gaussian distribution expected for single fluorophores (Figure 3C). By fitting a Gaussian function into the histogram, we obtain two populations of molecules with different fluorescence intensities that represent EGFP monomers and dimers, respectively (Figure 3C). The Gaussian function gives the mean (μ) and the variance (σ) for each population, which are in experiment 401,71 ± 118,67 fluorescence intensities for a single molecule (Figure 3C). In our system, single fluorophores are detectable at exposure times of 1s and above.
However, while imaging cells *in vivo* Vps4-3HA-EGFP goes into a complex of hexamer or dodecamers increasing the fluorescence intensity and sensitivity for our system in comparison to single molecule acquisition. Additionally, to assess dynamics while live cell imaging, it is crucial to acquire fast consecutive frames with quick interval times between frames. This fast acquisition is important to be able to track moving vesicles over time and not to lose them and thus to catch possible biological relevant events. Additionally, due to fast vesicle movement *in vivo*, high exposure times would increase the point-spread function of diffraction-limited objects dramatically. These objects would appear as elongated spots distort the detection and analysis.
To calculate from single molecule intensity values to lower exposure time e.g. 100ms for live cell imaging, we use the properties of EGFP that upon illumination, it emits proportional fluorescence intensity within a certain range under non-changing 488nm solid-state laser power (Cocucci et al., 2012). In particular, single molecule calibration were not only performed at 2s exposure but titrated with four different exposure times ranging from 1s to 2.5s with increasing 0.5s steps (Figure 3D). The mean values of each experiment were plotted in a graph on the y-axis whereas the respective exposure time was plotted on the x-axis (Figure 3D). By fitting a linear

regression to these data points, we obtain a linear regression equation (Figure 3D). In this way, we can calculate the specific fluorescence intensity for one molecule of EGFP for lower exposure times of 100ms.

4.3 The oligomeric state of Vps4 in the cytoplasm

Vps4 was previously reported to form dimers in the absence of ATP in solution in *in vitro* gel filtration experiments (Gonciarz et al., 2008). However, these experiments were performed at high protein concentrations of 150µM of Vps4 were used for gel filtration experiments which could alter protein assembly properties (Gonciarz et al., 2008). Thus, we wanted to confirm these results with a different experimental approach. Cells expressing Vps4-3HA-EGFP were treated *in vivo* with DMSO as a control and with the non-specific amine-reactive crosslinker Dithiobis[succinimidyl propionate] (DSP) to stabilize putative Vps4 dimer interfaces which are within close proximity of 12Å. Cells are then lysed and Vps4-3HA-EGFP proteins were immobilized on glass coverslips and detected by Spinning Disc Confocal microscopy (Figure 4A, 4C). Followed by subsequent computational analysis with custom-made Matlab scripts of single fluorophore bleaching steps in order to distinguish between populations of monomeric and dimeric molecules (Figure 4B, 4D).

Although the exact same amount of cells were used for both samples, the crosslinked lysis sample was diluted 1:5 before adding on the glass cover slip for proper detection by the tracking software. However, it still showed higher numbers of detected Vps4-3HA-EGFP molecules in comparison to the DMSO control suggesting a stabilization of Vps4 due to unspecific crosslinking (Figure 4A and 4C). By analyzing the histograms with of the amplitudes of single photo bleaching steps followed by the fitting of the Gaussian function, the DMSO control reveals one population of detected molecules resembling the pattern expected for single fluorophores suggesting one population of mainly monomers (Figure 4B). The cross-linked sample shows the same population of monomers in a Gaussian distribution (Figure 4D). Additionally, there is a tail in the histogram towards higher fluorescence intensities detectable indicating a second population with higher fluorescence intensities which could resemble a putative population of dimers (Figure 4D). These data suggest a monomer-dimer equilibrium of Vps4-3HA-EGFP *in vivo* rather than merely dimers in solution as previous publications suggested with *in vitro* experiments (Gonciarz et al., 2008).

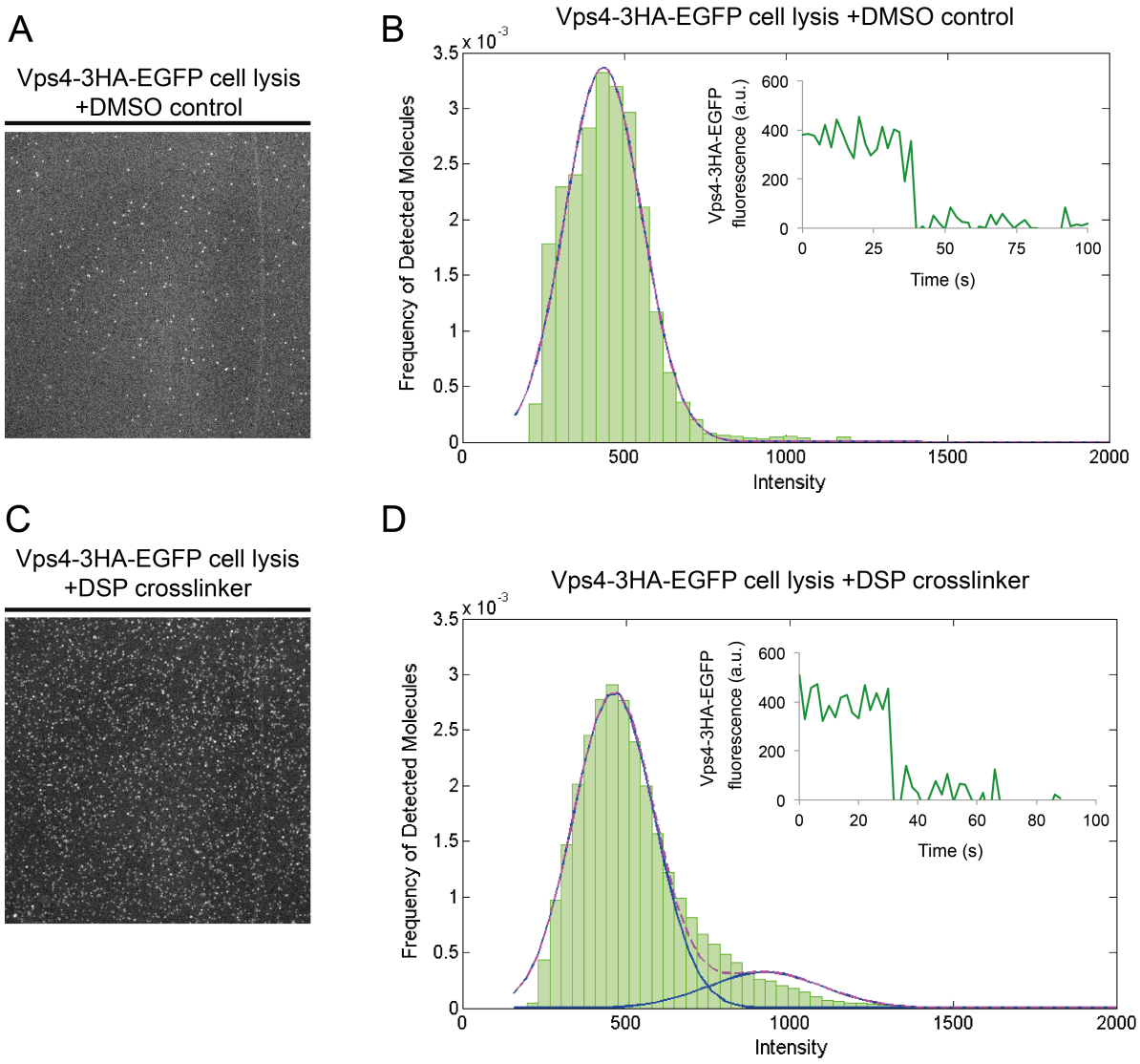

Figure 4. Vps4-3HA-EGFP cell lysis detected by Spinning Disc Confocal microscopy. A and C: Vps4-3HA-EGFP proteins treated with DMSO or DSP *in vivo* are immobilized on glass cover slips detected over at least 45 frames with an exposure time of 2s per frame. The DSP sample was diluted 1:5 due to high numbers of molecules. B and D: Tracings of single Vps4-3HA-EGFP molecules in the right top graph in B and D show representative photo bleaching steps of diffraction limited spots. The amplitudes of these steps were plotted as a histogram and show the Gaussian distribution expected for single fluorophores. The Gaussian fit reveals one population of single molecules in the DMSO control (B). A small second population appears in the DSP sample (D).

If any, just a small population of Vps4-3HA-EGFP dimerizes with crosslinker treatment suggesting the capability of Vps4 to form dimers if the dimer interface is stabilized. Further experiments are needed to support this new finding. Based on these results, gel filtration experiments from cell extracts could give new insights to the oligomeric state of Vps4 in solution.

4.4 Live cell imaging

4.4.1 The experimental setup

MVBs have typically the size of 150-200nm, thus these structures are smaller than the wavelength of the visible light (~ 500nm) resulting in detection of so called diffraction limited spots during fluorescent acquisition (Adell et al., 2014; Kural and Kirchhausen, 2012).

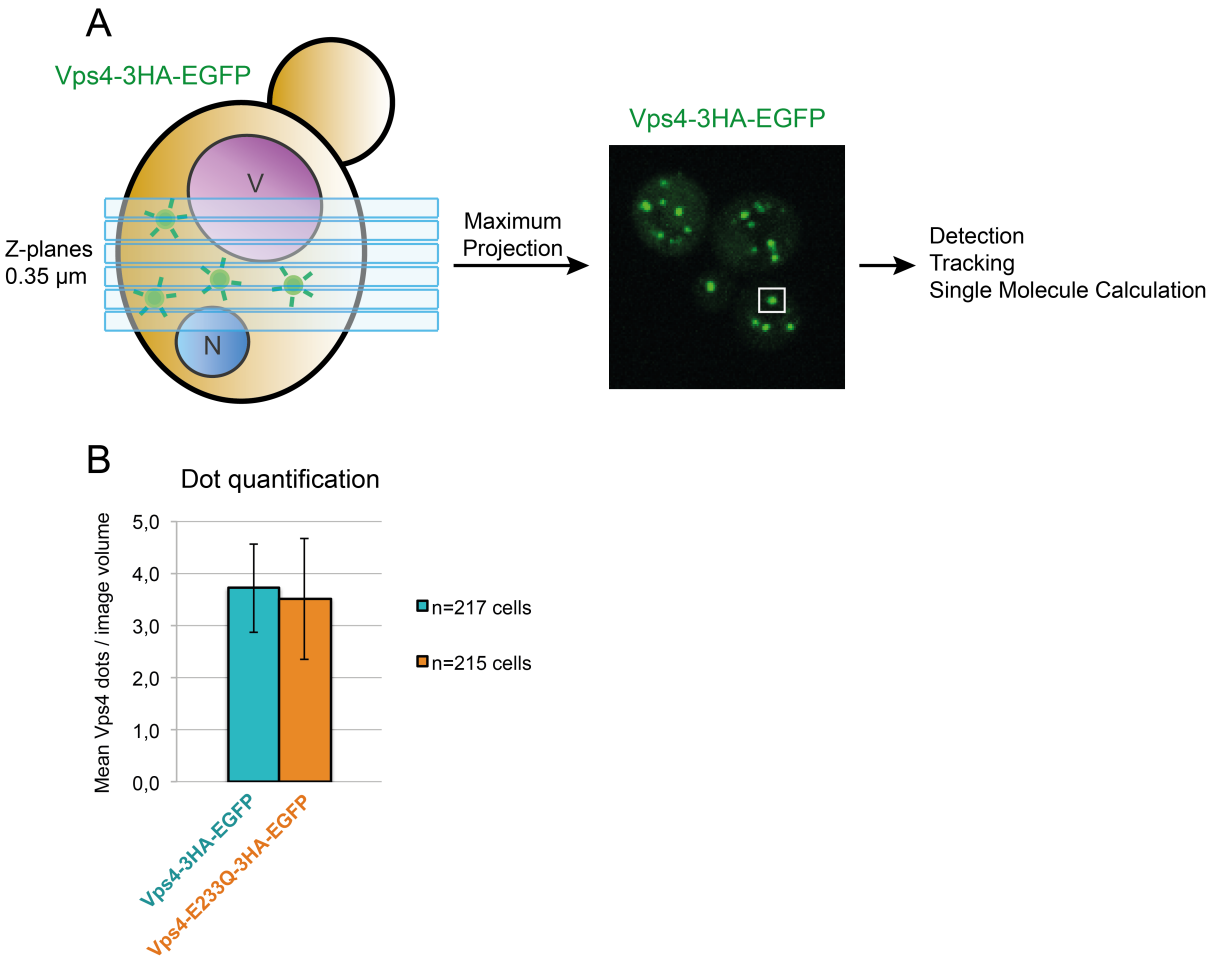

Figure 5A. Overview of the live-cell acquisition procedure by Spinning Disc Confocal microscopy. A: A schematic Vps4-3HA-EGFP yeast cell with nucleus (N) in blue and the vacuole (V) in magenta contains Vps4-3HA-EGFP positive vesicles detectable as diffraction limited spots. Six z-planes were acquired with a step size of 0.35 µm covering 2.1 µm of the cell. All planes were combined to a maximum z-projection for further detection, tracking and single molecule calculation (adapted from Kural et al., 2012). B: Quantification of mean detectable dots of cells expressing Vps4-3HA-EGFP (blue bar, n=217 cells) and Vps4-E233Q-3HA-EGFP (orange bar, n=215 cells).

Additionally, in order to fulfill their biological function such as cargo delivery to their destination, MVBs move extensively on actin cables within yeast cells (Moseley and Goode, 2006). This three dimensional movement of Vps4-3HA-EGFP positive vesicles increases the probability to lose vesicles in z-direction during acquisition. To solve this problem, we decided not only to acquire one plane but also acquire 6-7 z-stacks covering a volume of half of a yeast cell. However, there are limitations, which do not allow acquiring an infinite number of z-stacks.

(1) Mainly, the limitation of photo-bleaching: Organic fluorophores only emit a limited number of photons before their fluorescence diminishes (Kural and Kirchhausen, 2012). This results in a loss of signal upon extensive illumination (Kural and Kirchhausen, 2012). Consequently, acquiring more planes in order to cover the whole cell would photo-bleach Vps4-3HA-EGFP too fast for consecutive acquisition over time. (2) Increasing the number of z-planes during acquisition would ultimately increase the interval times between consecutive frames dramatically making it difficult to track vesicles over time. Due to these limitations, there has to be a 'trade-off' between the z-stack numbers, photo-bleaching and interval times. Here, we discovered the most efficient balance and decided to acquire 6-7 z-planes with a step size of 0.35 μm covering 2.1 – 2.45 μm of a cell (Figure 5A). Each plane is exposed for 100ms to ensure to be sensitive enough even for weak signals. After acquisition of all planes, the next subsequent frame is again acquired for typically 30 frames. In this way, a 4D image with variables x, y, z and t is generated. For further data detection, tracking and single molecule calculation, all planes are then combined by maximum z-projection to one 3D image consisting now of x, y and t (Figure 5A).

With these experimental settings, we assessed the mean Vps4 positive vesicles in Vps4-3HA-EGFP (WT) and Vps4-E233Q-3HA-EGFP (Vps4-EQ), a dominant negative ATPase deficient mutant, which cannot hydrolyze ATP and therefore constitutively interacts with the assembled ESCRT-III complex on endosomes (Figure 5B) (Babst, 1997). By quantifying 217 WT cells and 213 mutant cells, the results indicate that within a range of 2.1μm of the cells, which resembles approx. half of the cell, the mean number of dots detectable is 3,71 in WT and 3.51 in the mutant, thus shows no significant difference (Figure 5B). This goes in line with new unpublished data indicating the majority of Vps4 dots range from 1-7 detected dots per whole cell, rarely we can detect more than 7 Vps4 dots per cell (Migliano and Adell, unpublished data). These results show for the first time how many Vps4 positive MVBs exist in

yeast. Conclusively, yeast cells are able to promote the degradation of integral membrane proteins with less than 7 MVBs per cell.

4.4.2 Vps4-3HA-EGFP localizes to endosomes

The ESCRT machinery is recruited to endosomes in order to fulfill its function of cargo sorting and intraluminal vesicle formation (Teis et al., 2008). Here, we want to validate the proper localization of Vps4 to endosomes. By doing so, we used the lipophilic styryl dye FM4-64, which intercalates with the plasma membrane of the cell and thus emits red fluorescence. Through bulk endocytosis FM4-64 is then transported to endosomes and is further delivered via the MVB pathway to the vacuole. In this way it is possible to chase endocytic vesicles in Vps4-3HA-EGFP cells and assess the colocalization. Cells show proper Vps4-3HA-EGFP patterns indicated by numerous dots and cytoplasmic staining (Figure 6A, first panel). FM4-64 staining reveals moieties of red staining at the plasma membrane (Figure 6A, second panel). Additionally, dots are visible within the cells indicating endocytic vesicles (Figure 6A, second panel). The merge of Vps4-3HA-EGFP and FM4-64 reveals colocalization of some endocytic vesicles with Vps4 turning the signal to yellow (Figure 6A, third panel, white arrowheads). However, there are also vesicles detectable which do not colocalize with Vps4-3HA-EGFP (Figure 6A, third panel, magenta arrowsheads). To better detect colocalizing dots, we shifted the green channel to the right bringing colocalizing dots in close proximity in the x-axis whereas the originally single dots (magenta arrow) are not associated with a green dot to their right (Figure 6A, fourth panel). Two representative tracings show the simultaneous fluorescence signals of cololocalizing endocyctic vesicles (Figure 6B). The upper graph shows slight increase in Vps4-3HA-EGFP signals over time suggesting putative recruitment of Vps4 molecules whereas FM4-64 tracings indicate the fluorescence signal of the vesicle over time (Figure 6B, upper graph). The lower graph shows no dramatic change over time in both signals (Figure 6B, lower graph).

Since this is just a snapshot of a dynamic process of ESCRT recruitment and dissociation, it is possible that Vps4 negative vesicles either did not yet recruit Vps4 or Vps4 already disassembled. From these results, we conclude that Vps4-3HA-EGFP remains associated with endosomes for some time.

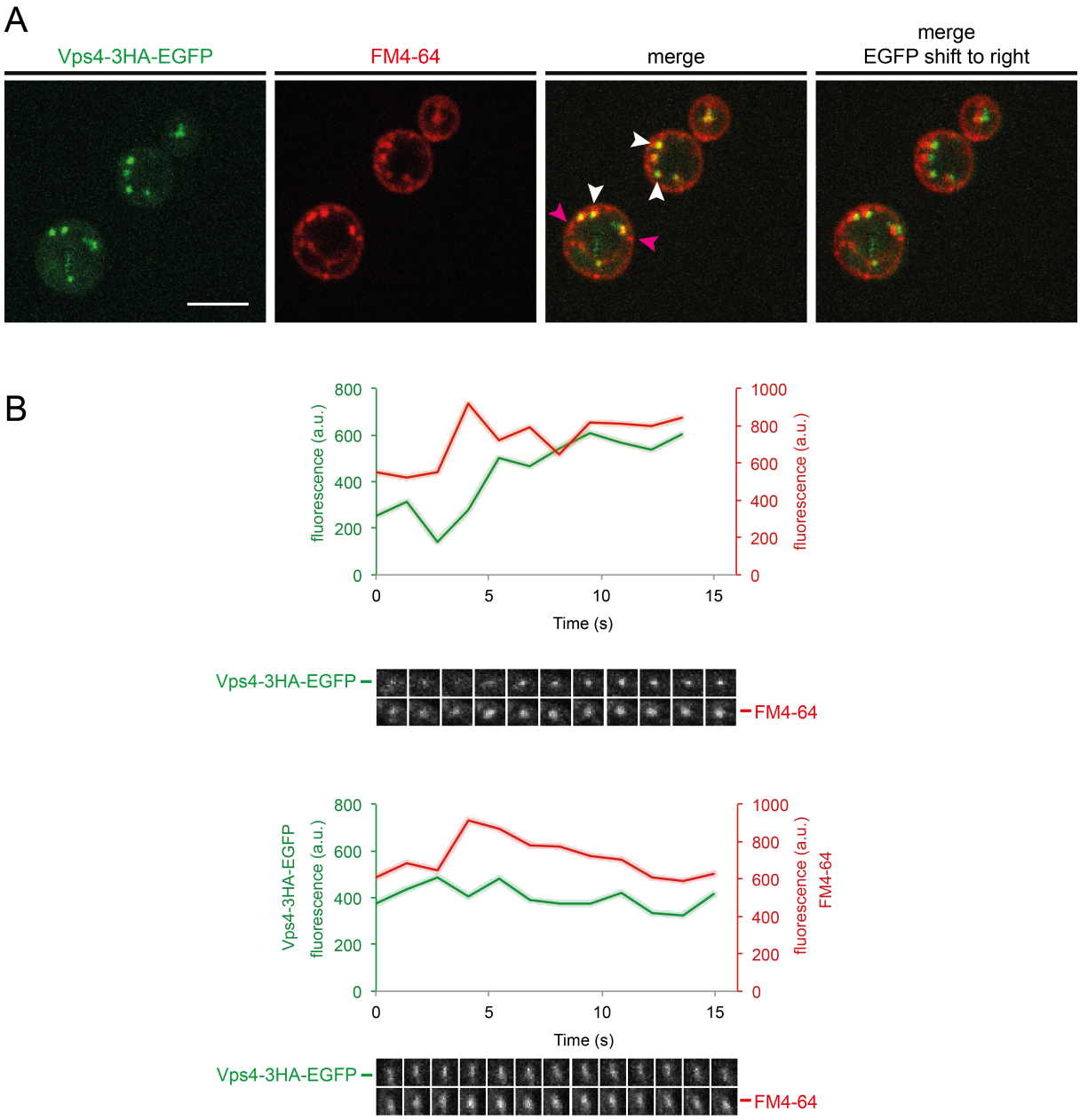

Figure 6. The lipophilic red fluorescence dye FM4-64 chased with Vps4-3HA-EGFP cells. A: Images are maximum projections of 5 planes with a 0.35 µm step size of Vps4-3HA-EGFP (green) chased with FM4-64 (red). Scale bar: 5 µm. EGFP channel was exposed for 50ms, red channel was exposed for 40ms. Vps4-3HA-EGFP shows dots and cytoplasmic signals. FM4-64 is detectable at the plasma membrane and on dots. The merged image shows colocalization of both (white arrowheads) but also Vps4 negative red dots (magenta arrowheads). EGFP channel is shifted to the right to facilitate the visibility of colocalization. B: Representative tracings of colocalizing Vps4-3HA-EGFP and FM4-64 dots are shown. Fluorescence intensities are given as arbitrary units.

4.4.3 Complex distribution analysis

We further analyzed the tracing data of WT Vps4-3HA-EGFP and the substrate trap mutant Vps4-E233Q-3HA-EGFP (Vps4-EQ) in order to assess preferential oligomeric states of Vps4 *in vivo*. Cells expressing wild type Vps4-3HA-EGFP show the expected pattern of dots within the cell and cytoplasmic fluorescent signals (Figure 6A, upper panel, magenta arrowheads). By comparing the mutant under the same imaging condition and the same dynamic range (min=1000, max=2000), we can detect the striking difference between the WT and Vps4-EQ. In particular, Vps4-E233Q-3HA-EGFP localizes to dots resulting in huge accumulations with high fluorescence intensities (Figure 8A, lower panel, white arrowheads). It is known that the expression of Vps4-EQ mutant induces a class-E phenotype, hence we conclude these accumulations to be class-E compartments (Shestakova et al., 2013). The fluorescence signal in the cytoplasm is decreased indicating the inability of the mutant to hydrolyze ATP and disassemble into the cytoplasm (Figure 7A, lower panel, magenta arrowheads). This finding goes in line with previous *in vivo* subcellular fractionation experiments in which Vps4-EQ localizes to the membrane fraction rather than being disassembled into the supernatant fraction (Adell et al., 2014). Additionally, Vps4-3HA-EGFP positive vesicles in the WT were very mobile, whereas the Vps4-3HA-E233Q-EGFP positive vesicles remained mostly static (data not shown).

To determine the number of Vps4-EGFP involved on diffraction-limited spots, we took in consideration all amplitudes of the first frame of each track and calculated fluorescence intensities to molecules by single molecule calibration. In this way, we can mostly exclude any aberrations due to photo-bleaching that could occur during consecutive illumination. These amplitudes were then analyzed by frequency distribution and were plotted as a histogram (Figure 7B). By binning the data to 18 classes with 6 molecules per class ranging from 6 to 96 molecules, we can detect high distribution of approx. 17% of the mutant complexes within the two first classes of 6 and 12 molecules, respectively (Figure 7B, left graph). Followed by a stepwise decrease of the complex distribution towards higher molecule classes (Figure 7B, left graph). By contrast, WT complexes show 9% distribution in the first class and peak with 18% at 12 molecules and subsequently show stepwise decreased distribution towards higher molecule complexes (Figure 7B, left graph). The minorities of WT complexes are detectable above 72 molecules whereas Vps4-EQ shows higher

distribution to 96 molecule classes (Figure 7B, left graph). In fact there is a portion of Vps4-E233Q-3HA-EGFP complexes bigger than 100 molecules and range up to 900 molecules which is explainable due to the inability of Vps4-E233Q-3HA-EGFP to hydrolyze ATP and hence traps on class-E compartments by binding constitutively to ESCRT-III complexes (Figure 7B, right graph). However, no WT molecules are higher than 96 molecules suggesting Vps4 ultimately dissociate from the ESCRT-III complex. High molecule number complexes could be accumulation of several MVBs in close proximity to each other. These MVB clusters are still detectable as diffraction-limited spots and cannot be distinguished of single MVBs and therefore are possibly detected as higher molecule numbers. Next, we binned all complexes of the WT and mutant, which appear within 1-50 molecules in 50 classes (Figure 7C and 7D). Unexpectedly, we cannot detect clear peaks of complexes with a factor of 6, rather there is a general broad distribution of the complexes (Figure 7C and 7D). However, in both, the WT and the Vps4-E233Q-3HA-EGFP mutant, we can clearly detect the highest peak at 6 molecules indicating that Vps4 could initially assemble into a hexameric complex and then either is already functional as a hexamer or subsequently assemble into a higher complex in order to fulfill its function (Figure 7C and 7D).

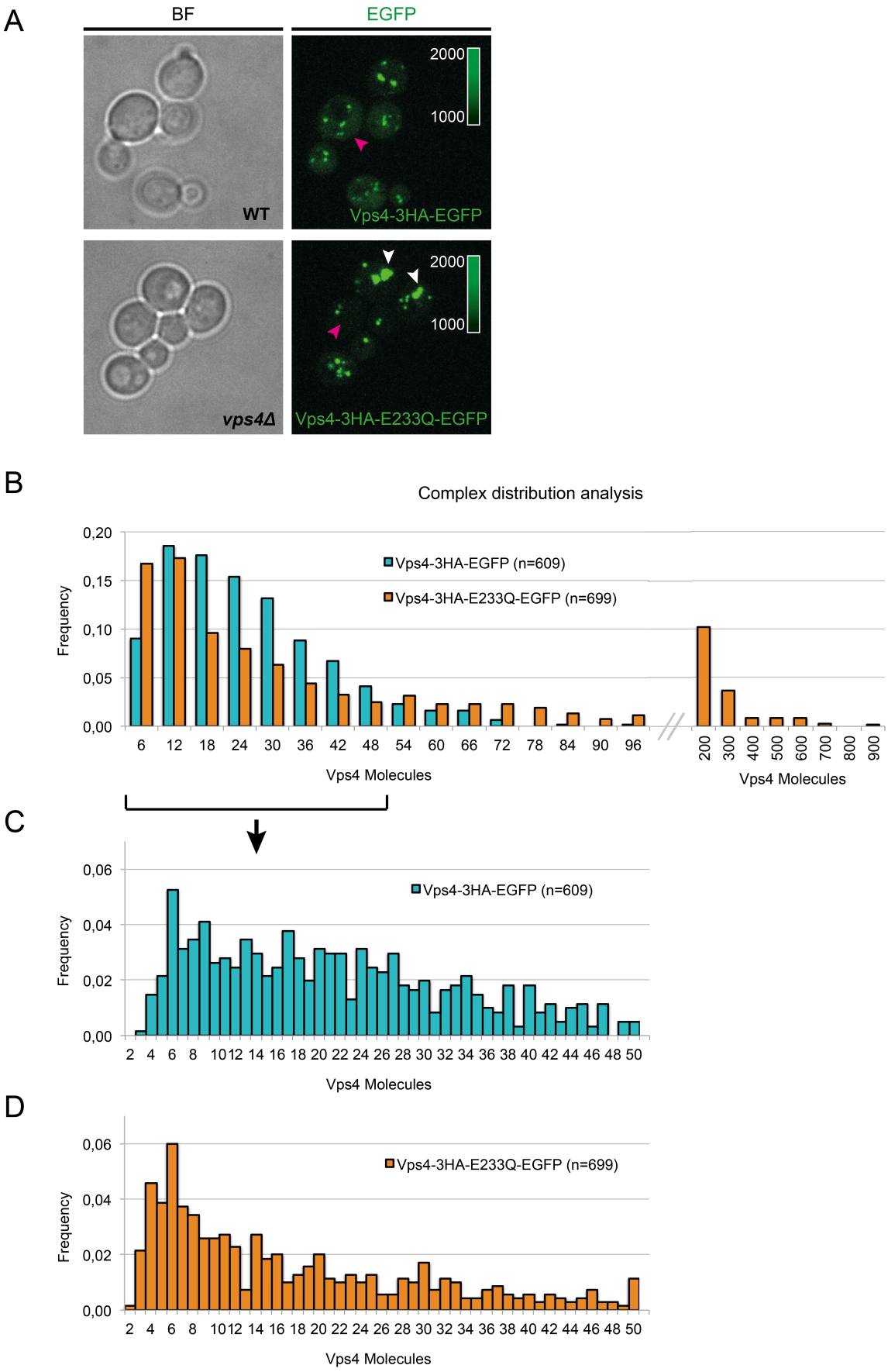

Figure 7. Complex distribution analysis of Vps4-3HA-EGFP and Vps4-E233Q-3HA-EGFP. A: Images show brightfield (BF) and fluorescent acquisition of EGFP (EGFP) of chromosomal integrated Vps4-3HA-EGFP (upper panel) and *vps4Δ* cells expressing Vps4-E233Q-3HA-

EGFP under an endogenous promoter (lower panel). 6-7 planes were exposed for 100ms each and were maximum projected. The dynamic range is adjusted from 1000 to 2000 in both images. Vps4-3HA-EGFP shows dots and cytoplasmic signal (magenta arrowheads). Vps4-E233Q-3HA-EGFP mutant shows higher fluorescent signals in class-E compartments (white arrows). Cytoplasmic signal in the mutant is decreased compared to WT (magenta arrowheads). B: Frequency analysis of the amplitudes of the first frame of each track calculated to molecule numbers were plotted as a histogram with 16 bins with classes of 6 molecules. All complexes higher than 96 molecules were combined in 8 classes consisting of 100 for each class. C and D: complexes of WT and mutant within 50 molecules were plotted as a histogram consisting of 50 classes of single molecules. The data was normalized to total counted complexes for WT and mutant, respectively and indicated as frequency.

4.4.4 Single molecule tracking analysis

Next, we analyzed Vps4-3HA-EGFP (WT) cells by live cell imaging as described in 3.4.1 and normalized fluorescence intensities of tracings to molecule numbers as described above in 3.2. In order to see the impact of dynamic Vps4 assembly and disassembly, we decided to compare Vps4-3HA-EGFP to the ATPase deficient mutant Vps4-E233Q-3HA-EGFP (Figure 8A).

Representative tracings of WT Vps4-3HA-EGFP normalized to their molecule numbers show dynamic changes in their molecule numbers over time (Figure 8A). The left upper tracing graph shows distinct patterns starting at ~12 molecules followed by a quick burst to ~18 molecules and rather slow decay over approx. 8 seconds to again 12 molecules could indicate a Vps4 disassembly event (Figure 8A, left upper graph). This putative event is subsequently repeated twice until the signal stepwise decreases to 6 molecules (Figure 8A, left upper graph). This particular case would indicate Vps4 monomers/dimers to be recruited rapidly to the complex, or to another ESCRT-III site on the same endosome, fulfilling its function of membrane scission and ESCRT-III disassembly resulting in its stepwise dissociation from the membrane over 5-10 seconds.

However, these tracings alone cannot precisely confirm this suggestion and therefore further experiments are required to assess this assumption. Typically tracings are often associated within the range of 6-40 molecules. Rarely they show more than 50 molecules (Figure 7 and data not shown). By contrast to WT tracings, Vps4-EQ shows strikingly different tracing patterns (Figure 8B). In particular, tracings start typically at a certain molecule number e.g. 6, ~20, ~18 and ~12 and decay due to photo-bleaching over time. No exchange of new incoming Vps4 molecules nor dissociation could be observed since Vps4-EQ cannot hydrolyze ATP and is locked as a complex (Figure 8B).

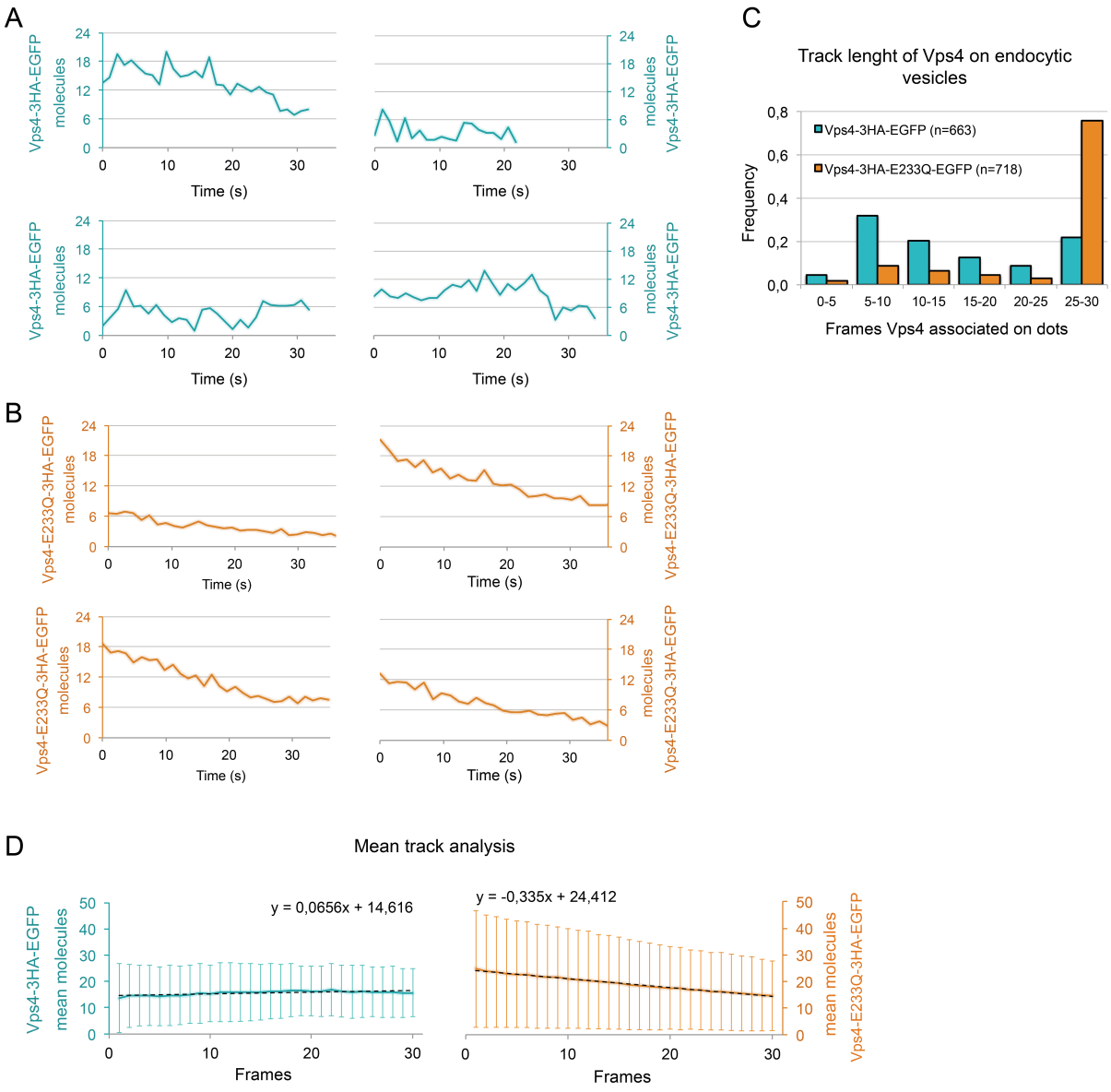

Figure 8. Single molecule tracking analysis of Vps4-3HA-EGFP and ATPase deficient mutant Vps4-E233Q-3HA-EGFP. A and B: Representative tracings of Vps4-3HA-EGFP (blue) and Vps4-E233Q-3HA-EGFP (orange) normalized to single molecules. WT tracings show dynamic increases and decreased of Vps4 molecules over time. Mutant tracings show no dynamic increases but show strong decay over time. C: Histogram shows the frequency of the track length Vps4 associated on dots in frames of WT (blue bars) and mutant (orange bars). E: Mean molecule numbers and their variance of each frame of WT (blue left graph) and mutant (orange right graph) were plotted. In the mutant, all tracings higher than 96 molecules were excluded for better comparison to WT. The linear regression line fitted to the data gives the regression equation. The slope is positive for WT and negative for the mutant.

Interestingly, Vps4-E233Q-3HA-EGFP is often detectable at its starting point as a complex number with a factor of 6 validating the current model of Vps4 appearing as a functional hexameric or dodecameric complex (Figure 8B, Figure 7 and Monroe et al., 2014).

Furthermore, we analyzed the track length of Vps4 on endocytic vesicles. Therefore we performed a frequency analysis of the length of 663 WT and 718 mutant tracings to determine how long we could track Vps4-3HA-EGFP and Vps4-EQ. Due to technical reasons and photo-bleaching effects we took in consideration a window of a minimum of 5 frames and a maximum of 30 frames, therefore it is possible that some tracings would show even longer association than 30 frames. Each frame has an interval time of 1.0 – 1.3s depending on the particular image. The results were plotted as a histogram and normalized to 1 (total tracings) on the y-axis (Figure 8C). Strikingly, we can detect a broader distribution of the track length of WT Vps4 (blue bars) in contrast to the mutant (Figure 8C, orange bars). The highest fraction of the WT is detectable between 5-10 frames indicating shorter tracings associated with Vps4 suggesting a faster dissociation of Vps4 (Figure 8C). By contrast, Vps4-E233Q-3HA-EGFP shows the highest distribution at 25-30 frames indicating non-dynamic long-term accumulations of the mutant protein consequently little is distributed to smaller fractions (Figure 8C). However, we cannot entirely rule out the possibility that some short-term associated vesicles are simply lost due to z-movement.

To further assess differences between Vps4-3HA-EGFP and Vps4-EQ, we plotted the average of molecules and their respective variances of tracings for each frame in the WT (n=663, blue left graph) and the mutant (n=588, orange right graph, Figure 8D). To better compare both genotypes, we excluded in the mutant all tracings showing higher molecule numbers than 96 since these are the highest molecule numbers detectable in the WT and would resemble aggregations in class-E compartments (Figure 7). By plotting the average of each frame and its variance and fitting a linear regression line and its equation, we can assess the tendency of the WT tracks in comparison to the mutant. The WT starts with an average of 13.58±13.17 molecules at the first frame and even raises slightly over time indicated by the positive slope of 0.0656x (Figure 8D). By contrast, the mean Vps4-E233Q-3HA-EGFP tracing starts much higher at 24.67±21.88 indicating the higher number of molecules accumulating in this mutant (Figure 8D). Additionally, the fluorescence decays indicated by the negative slope of -0.335x suggesting rather no addition of new Vps4 molecules over time compared to WT (Figure 8D). These results verify our findings from the

representative tracings and consolidate the dataset consisting of 663 WT tracks and 588 mutant tracks.

All in all, by showing typical increases and decreases in molecule numbers, a broad distribution of shorter residency times of Vps4 associated on endocytic vesicles and higher relative changes in molecule numbers in comparison to the mutant could confirm the high dynamic properties of Vps4.

5 Discussion

Vps4 is involved in all ESCRT-III membrane scission steps, like cytokinesis, HIV and ILV budding (Adell and Teis, 2011). Furthermore it is now clear that Vps4 by its coordinated binding to Snf7 and Vps2 and thus couples ESCRT-III disassembly to membrane neck constriction (Adell et al., 2014). However, to present date the kinetics and the dynamic properties of Vps4 remain unknown.

Here, we assess these questions for the first time by live-cell single molecule imaging and subsequent computational analysis. Thereby we can detect that Vps4 colocalizes to endocytic vesicles and therefore is properly recruited to the endocytic pathway (Figure 6). However, depending on the time window of the FM4-64 chase, there were also Vps4 negative vesicles detectable which are probably either in transition of maturation or not yet recruited by Vps4 (Figure 6).

By analyzing cell lysis of Vps4-3HA-EGFP cells, we could reveal one population of monomeric Vps4 (Figure 4A). By adding *in vivo* an non-specific crosslinking reagent we could stabilize a small population of dimers indicating the ability of Vps4 to dimerize in advance of its oligomerization into a functional complex but preferentially occurs as a monomer in the cytosol (Figure 4A and 4B). Our data goes in line with previous publications assessing the *in vivo* oligomeric state of mammalian Vps4 by a different approach called image correlation spectroscopy (ICS) (Baumgärtel et al., 2011). However, other publications from structural *in vitro* experiments suggested Vps4 to appear as dimers in solution in the absence of ATP (Gonciarz et al., 2008). These *in vitro* experiments were performed with high protein concentrations of 150µM that could alter protein assembly properties. Therefore we conclude from our experiments Vps4 preferentially to appear as a monomer in solution.

We further could reveal dynamic tracings of Vps4 showing bursts of increases and decreases in molecule numbers, whereas the substrate trap mutant Vps4-E233Q-3HA-EGFP did not show dynamic changes, rather showed a decay in molecule numbers due to photo-bleaching (Figure 8A and 8B). This decay of Vps4-E233Q-3HA-EGFP tracings suggests no incoming new Vps4 molecules to the complex rather than the photo-bleaching of existing proteins. This in turn suggests a high turnover of Vps4 molecules within WT complexes because very little, if any photo-bleaching is detectable in WT tracings (Figure 8A). These results indicate a strong exchange in wild type Vps4 subunits and could further be confirmed with Fluorescence Recovery

after Photobleaching (FRAP) experiments in the future. By photo-bleaching a certain area of the cell and comparing the recovery times of Vps4 to dots in the WT and the mutant, we would expect a significant faster recovery of Vps4 to endocytic vesicles in the WT compared to the Vps4-EQ.

From our tracing data, we detect typically detect short peaks and immediate decay within 5-10 seconds (Figure 8A). This burst pattern generally goes in line with previous experiments where the authors assessed Vps4 involvement in HIV budding in mammalian cells (Baumgärtel et al., 2011). However, they found the association of this burst for an average of ~35s (Baumgärtel et al., 2011). This difference could be explained because the HIV machinery highjacks cellular components of ESCRT and Vps4 to the site of HIV budding and is recruited to a different location, the plasma membrane for vesicle budding outwards of the cell, hence the scission reaction could undergo a different progression and therefore could prolong longer than in our experiments (Bleck et al., 2014). The main question still remains, whether these bursts shown in our experiments equal exactly one scission ILV budding event or is there a contribution of many Vps4 bursts in order to accomplish one ILV scission event.

We could further show the dynamic properties of Vps4 by comparing track lengths of our tracing data of WT and mutant Vps4 (Figure 8C). Particularly, WT Vps4 showed a broader distribution of the track length time suggesting a fraction of Vps4 complexes dissociating after a shorter time period from the vesicles rather than accumulating for long time periods on class-E compartments as shown for the Vps4-E233Q-3HA-EGFP mutant (Figure 8C). HIV budding experiments showed and average burst time of ~35s of Vps4 (Baumgärtel et al., 2011). Generally, our data suggests the track length time to be evenly distributed from 5 (approx. 6s) to 30 (approx. 36s) frames, indicating also short-term association on endocytic vesicles (Figure 8C). However, short-term vesicles could already be associated with Vps4 for a longer time period in advance of acquisition. Long-term Vps4 positive vesicles could resemble more mature vesicles or vesicle clusters as previously shown. In fact, long-term vesicles are preferentially localized to the border of the vacuole, whereas transient vesicles in the cell periphery are more motile (data not shown). Therefore we conclude that WT Vps4 ultimately dissociates from the endosomes, whereas Vps4-EQ remains associated on endosomes. However, we cannot entirely rule out the possibility that a fraction of these shorter frames are due to their z-direction movement and are lost during the tracking analysis.

By analyzing the complex distribution of Vps4 complexes, we could show that 82.59% WT Vps4 were distributed from 6-36 molecules indicating the majority of detected dots form complexes of 1-6 hexamers. By contrast, 62.37% of Vps4-EQ is distributed from 6-36 molecules. Additionally, Vps4-EQ shows aggregations of high molecule number complexes ranging from 100 – 900 molecules, which resemble the class-E compartments (Figure 7B). By narrowing down the classes, we can detect certain peaks in classes with the factor of 6 molecules, but unexpectedly could not detect clear separations between hexamer or dodecamer complexes, but rather there are broad classes of complexes distributed between these peaks (Figure 7C). The broad distribution could be explained either due to technical reasons, because exciting EGFP continuously results in variance in its amplitude. Consequently, the single molecule calibration results in a variance of the single molecule intensity that is typically 26-30%. By acquiring an EGFP fusion protein within a complex, the general error could add up due to excitement of many EGFP molecules fused to the protein of interest. The other possibility could lie in a biological explanation that Vps4 produces intermediate complexes until it fully assembled into its functional unit, putatively a hexamer or dodecamer. Again during HIV budding in mammalian cells, previous publications suggested an average of two to five dodecamers to be involved during the scission step (Baumgärtel et al., 2011). However, these experiments were performed in ~20 to 40 fold EGFP-Vps4 overexpression over endogenous levels (Baumgärtel et al., 2011). Although they performed control experiments and state that the overexpression of Vps4 does not affect its functionality, the number of recruited molecules to highjacked ESCRT complexes may increase due to the vast number of Vps4 molecules in the cytoplasm (Baumgärtel et al., 2011). Our experiments were performed with chromosomal integrated strains specific knockout strains complemented with vectors under endogenous promoters to ensure endogenous expression levels and full exchange of the native protein with the EGFP-tagged version. Regarding the complex distribution, our data suggests the ability of Vps4 to form a complex as a hexamer (Figure 7C). However, we cannot rule out the possibilities that these hexamers are solely functional, or they require a recruitment of an additional hexamer to assemble into a functional super-complex with its co-factor Vta1 (Azmi, 2006; Xiao et al., 2008). Future tracking analysis of Vps4-3HA-EGFP in *vta1Δ* cells could assess whether Vta1 is required for Vps4 complex assembly and how missing Vta1 affects Vps4 burst patterns.

Finally, we can conclude from our data, that from 609 analyzed wild type Vps4 complexes, the minority shows more than 36 molecules per vesicle suggesting a maximum of six Vps4 hexamers assemble on one or a cluster of MVBs at the same time. Our data suggest Vps4 to be recruited as monomers or dimers to form hexamers. Either Vps4 hexamers are already functional and are recruited to different assembly sites on endosomes, or many hexamers are required for one scission event.

Conclusively, by using Spinning Disc Confocal microscopy and live-cell single molecule imaging we could set up an acquisition system for baker's yeast in order to identify the oligomeric state of Vps4 in the cytoplasm, its dynamic properties over time and its preferential complex distribution. In this way, we contributed with this project for the first time to the understanding of dynamics of the ESCRT machinery during ILV biogenesis *in vivo*.

6 Materials and Methods

6.1 Strains and Plasmids

Strain	Name	Genotype	Source
SEY6210.1	WT	Mat a leu2-3,112 ura4-52 his3-Δ200 trp1-Δ901 lys2-801 suc2-Δ9	(Robinson et al., 1988)
MBY4	vps4Δ	SEY6210, VPS4::TRP1	(Babst et al., 2002a)
PPY12	Vps36-GFP	SEY62010, VPS36-GFP::HIS3	this study
DKY54	Vps23-GFP	SEY62010, VPS23-GFP::HIS3	(Katzmann et al., 2001)
MAY140	Vps4-3HA-EGFP	SEY6210, Vps4-3HA-EGFP::TRP1	this study

Table 1. List of strains used in this work.

Plasmids	Description	Source
pMB343	pRS416, Vps4-E233Q-3HA-EGFP	this study

Table 2. List of plasmids used in this work.

6.2 Fluorescence microscopy

Fluorescence microscopy was previously described (Adell et al., 2014). For live-cell microscopy, cells were grown to midlog (OD_{600} = 0.6) at RT in yeast nitrogen base (fluorochromes used in this study were GFP, EGFP, mCherry) and labeled with FM4-64 (Invitrogen) as previously described (Teis et al., 2008). Fluorescence microscopy was performed with a microscope (Axio Imager.M1; Carl Zeiss) and an α-Plan Fluar 100x, 1.45 NA oil objective (Carl Zeiss). Images were taken with a charge-coupled device camera (Spot Explorer, Visitron Systems). Acquisition software used was VisiView 2.0.3 (Visitron Systems). Image channels and merge imaged were created and brightness and contrast was enhanced in the RGB channel using ImageJ 1.47v.

6.3 Spinning Disc Confocal microscopy

6.3.1 Glass Coverslip Preparation

Glass coverslips were prepared as previously described (Cocucci et al., 2012). Glass coverslips (#1.5, Warner Instruments, Hamden, CT) were cleaned by sonication (Branson, Danbury, CT) for 30 min and were dried at 120°C. For Single molecule preparation cleaned coverslips were exposed to air plasma inside a glow discharge unit (Electron Microscopy Science, Hatfield, PA) operated at 30 mA, negative charge for 5 min.

6.3.2 Yeast Mounting

For live-cell microscopy, cells were grown in selective Yeast Nitrogen Base media to midlog (OD_{600} = 0.6), washed 2x in sterile aqua dest. and resuspended in 100µl aqua dest. Low melting agarose was diluted to 2% (Lonza NuSieve GTG Agarose) in selective Yeast nitrogen base medium was prepared by dissolving at 65°C, vortexing and keeping liquid at 40°C. 1 volume was added to cells to achieve a final concentration of 1% and vortexed briefly. 6µl of the cells-low melting agarose mix was added to coverslips and immediately covered by a second coverslip (18mm diameter) spreading the cell suspension and incubated for 5min at RT. The coverslip was mounted on a sample holder.

6.3.3 Microscopes

Spinning disk confocal fluorescence microscopy was performed as previously described (Cocucci et al., 2012). The MarianaTD system made of a computer-controlled inverted microscope (Axiovert 200M, Carl Zeiss, Thornwood, NY) equipped with a 100x objective (Plan-Apochromat, NA 1.49, Zeiss), a spinning disk confocal head (CSU-XI, Yokogawa Electric Corporation, Sugar Land, TX) and a spherical aberration correction system (Infinity Photo-Optical, Boulder,CO). Excitation light was provided by a 488 nm solid-state laser (Saphire, 50 mW, Coherent Inc, Santa Clara, CA) coupled to an acousto-optical tunable filter. Images were obtained with 100 ms exposures using a cooled CCD camera (QuantEM, 512SC, Photometrics, Tucson, AZ) under control of Slidebook acquisition software (Intelligent Imaging Innovations).

6.3.4 Single Molecule Calibration

10ml 1x PBS was prepared at RT. 10ml milli-Q water was prepared and 1µl of 0.1µm yellow-green 505/515 Fluo Spheres (Invitrogen) were added. Recombinant EGFP was diluted 1:10.000 in 1x PBS, Vps4-3HA-EGFP supernatants from cell lysis was analyzed undiluted. 1µl 1:10.000 Fluo Spheres were added to 100µl 1:10.000 EGFP or cell lysis. After pipetting up and down and the mixed solution was added directly in the center of a cleaned and plasma treated, negatively charged coverslip and incubated in the dark for 5min at RT. Residual solution at the edges of the coverslip were cleaned with a Kim Wipe. The coverslip was mounted in a sample holder and 1ml room temperature warm 1x PBS was added carefully at the wall of the sample holder and not directly onto the coverslip. Fluo Spheres were found by 20ms exposure times continuous streaming and focused for their maximum intensity in order to find the best plane. The filed of view was changed to loose the Fluo Spheres signal and EGFP molecules were acquired with 1, 1.5, 2 and 2,5s exposure times in different fields of view. At least 3-5 different images were acquired of each exposure time in order to calculate the linear regression of the single molecule calibration.

6.4 In vivo crosslinking

Subcellular fractionation of proteins into membrane-associated pellets and soluble cytoplasmic fractions was performed as previously described (Adell et al., 2014; Babst, 1997). In vivo DSP crosslinking procedure was adapted from (Copic et al., 2007). 30 OD_{600} equivalents of the yeast cells grown to mid-log phase (OD = 0.6) were spheroblasted, washed in crosslinking buffer (20mM HEPES pH 7.4; 0.7M Sorbitol; 100mM KOAc; sterile filtered) and resuspended in 5ml crosslinking buffer. 5mM DSP (dissolved in DMSO) was added shook 30min at RT. The crosslinking reaction was quenched with 100mM Tris,pH 7.4 and incubated for 15min at RT. Cells were then resuspended in 300µl ice cold PBS (+protease inhibitors) and homogenized by douncing. After a clearing spin (500g for 5min), supernatans were centrifuged (15.000g for 10min) to separate heavy membranes from cytosol. The supernatand was snap freezed and stored at -80 for subsequent acquisition.

6.5 Image Analysis

All image analysis were performed via Matlab (MathWorks, Natick, MA), using published and modified cmeAnalysis software as previously described (Aguet et al., 2013; Cocucci et al., 2012). The basic software package used in this work is available for download at: http://lccb.hms.harvard.edu/software.html. For further tracking, filter and single molecule calibration scripts, please contact the author.

7 References

Adell, M.A.Y., Vogel, G.F., Pakdel, M., Muller, M., Lindner, H., Hess, M.W., and Teis, D. (2014). Coordinated binding of Vps4 to ESCRT-III drives membrane neck constriction during MVB vesicle formation. The Journal of Cell Biology *205*, 33–49.

Adell, M.A.Y., and Teis, D. (2011). Assembly and disassembly of the ESCRT-III membrane scission complex. FEBS Letters *585*, 3191–3196.

Aguet, F., Antonescu, C.N., Mettlen, M., Schmid, S.L., and Danuser, G. (2013). Advances in Analysis of Low Signal-to-Noise Images Link Dynamin and AP2 to the Functions of an Endocytic Checkpoint. Developmental Cell *26*, 279–291.

Azmi, I. (2006). Recycling of ESCRTs by the AAA-ATPase Vps4 is regulated by a conserved VSL region in Vta1. The Journal of Cell Biology *172*, 705–717.

Babst, M. (1997). Endosomal transport function in yeast requires a novel AAA-type ATPase, Vps4p. The EMBO Journal *16*, 1820–1831.

Babst, M. (1998). The Vps4p AAA ATPase regulates membrane association of a Vps protein complex required for normal endosome function. The EMBO Journal *17*, 2982–2993.

Babst, M., Katzmann, D.J., Estepa-Sabal, E.J., Meerloo, T., and Emr, S.D. (2002a). Escrt-IIIAn endosome-associated heterooligomeric protein complex required for mvb sorting. Developmental Cell *3*, 271–282.

Babst, M., Katzmann, D.J., Snyder, W.B., Wendland, B., and Emr, S.D. (2002b). Endosome-Associated Complex, ESCRT-II, Recruits Transport Machinery for Protein Sorting at the Multivesicular Body. Developmental Cell *3*, 283–289.

Bache, K.G. (2006). The ESCRT-III Subunit hVps24 Is Required for Degradation but Not Silencing of the Epidermal Growth Factor Receptor. Molecular Biology of the Cell *17*, 2513–2523.

Baumgärtel, V., Ivanchenko, S., Dupont, A., Sergeev, M., Wiseman, P.W., Kräusslich, H.-G., Bräuchle, C., Müller, B., and Lamb, D.C. (2011). Live-cell visualization of dynamics of HIV budding site interactions with an ESCRT component. Nature Cell Biology *13*, 469–474.

Bleck, M., Itano, M.S., Johnson, D.S., Thomas, V.K., North, A.J., Bieniasz, P.D., and Simon, S.M. (2014). Temporal and spatial organization of ESCRT protein recruitment during HIV-1 budding. Proceedings of the National Academy of Sciences *111*, 12211–12216.

Carlton, J.G., and Martin-Serrano, J. (2007). Parallels Between Cytokinesis and Retroviral Budding: A Role for the ESCRT Machinery. Science *316*, 1908–1912.

Cocucci, E., Aguet, F., Boulant, S., and Kirchhausen, T. (2012). The First Five Seconds in the Life of a Clathrin-Coated Pit. Cell *150*, 495–507.

Cocucci, E., Gaudin, R., and Kirchhausen, T. (2014). Dynamin recruitment and membrane scission at the neck of a clathrin-coated pit. Molecular Biology of the Cell *25*, 3595–3609.

Copic, A., Starr, T.L., and Schekman, R. (2007). Ent3p and Ent5p Exhibit Cargo-specific Functions in Trafficking Proteins between the Trans-Golgi Network and the Endosomes in Yeast. Molecular Biology of the Cell *18*, 1803–1815.

Davies, B.A., Azmi, I.F., Payne, J., Shestakova, A., Horazdovsky, B.F., Babst, M., and Katzmann, D.J. (2010). Coordination of Substrate Binding and ATP Hydrolysis in Vps4-Mediated ESCRT-III Disassembly. Molecular Biology of the Cell *21*, 3396–3408.

Ferguson, S.M., and De Camilli, P. (2012). Dynamin, a membrane-remodelling GTPase. Nature Reviews Molecular Cell Biology.

Gonciarz, M.D., Whitby, F.G., Eckert, D.M., Kieffer, C., Heroux, A., Sundquist, W.I., and Hill, C.P. (2008). Biochemical and Structural Studies of Yeast Vps4 Oligomerization. Journal of Molecular Biology *384*, 878–895.

Henne, W.M., Buchkovich, N.J., and Emr, S.D. (2011). The ESCRT Pathway. Developmental Cell *21*, 77–91.

Henne, W.M., Buchkovich, N.J., Zhao, Y., and Emr, S.D. (2012). The Endosomal Sorting Complex ESCRT-II Mediates the Assembly and Architecture of ESCRT-III Helices. Cell *151*, 356–371.

Huang, F., Kirkpatrick, D., Jiang, X., Gygi, S., and Sorkin, A. (2006). Differential Regulation of EGF Receptor Internalization and Degradation by Multiubiquitination within the Kinase Domain. Molecular Cell *21*, 737–748.

Im, Y.J., Wollert, T., Boura, E., and Hurley, J.H. (2009). Structure and Function of the ESCRT-II-III Interface in Multivesicular Body Biogenesis. Developmental Cell *17*, 234–243.

Katzmann, D.J., Babst, M., and Emr, S.D. (2001). Ubiquitin-Dependent Sorting into the Multivesicular Body Pathway Requires the Function of a Conserved Endosomal Protein Sorting Complex, ESCRT-I. Cell *106*, 145–155.

Kirchhausen, T., Owen, D., and Harrison, S.C. (2014). Molecular Structure, Function, and Dynamics of Clathrin-Mediated Membrane Traffic. Cold Spring Harbor Perspectives in Biology *6*, a016725–a016725.

Kural, C., and Kirchhausen, T. (2012). Live-Cell Imaging of Clathrin Coats. In Methods in Enzymology, (Elsevier), pp. 59–80.

Kural, C., Tacheva-Grigorova, S.K., Boulant, S., Cocucci, E., Baust, T., Duarte, D., and Kirchhausen, T. (2012). Dynamics of Intracellular Clathrin/AP1- and Clathrin/AP3-Containing Carriers. Cell Reports *2*, 1111–1119.

Monroe, N., Han, H., Gonciarz, M.D., Eckert, D.M., Karren, M.A., Whitby, F.G., Sundquist, W.I., and Hill, C.P. (2014). The Oligomeric State of the Active Vps4 AAA ATPase. Journal of Molecular Biology *426*, 510–525.

Moseley, J.B., and Goode, B.L. (2006). The Yeast Actin Cytoskeleton: from Cellular Function to Biochemical Mechanism. Microbiology and Molecular Biology Reviews *70*, 605–645.

Robinson, J.S., Klionsky, D.J., Banta, L.M., and Emr, S.D. (1988). Protein sorting in Saccharomyces cerevisiae: isolation of mutants defective in the delivery and processing of multiple vacuolar hydrolases. Molecular and Cellular Biology *8*, 4936–4948.

Rodahl, L.M., Haglund, K., Sem-Jacobsen, C., Wendler, F., Vincent, J.-P., Lindmo, K., Rusten, T.E., and Stenmark, H. (2009). Disruption of Vps4 and JNK Function in Drosophila Causes Tumour Growth. PLoS ONE *4*, e4354.

Schmidt, O., and Teis, D. (2012). The ESCRT machinery. Current Biology *22*, R116–R120.
Shestakova, A., Curtiss, M., Davies, B.A., Katzmann, D.J., and Babst, M. (2013). The Linker Region Plays a Regulatory Role in Assembly and Activity of the Vps4 AAA ATPase. Journal of Biological Chemistry *288*, 26810–26819.

Teis, D., Saksena, S., and Emr, S.D. (2008). Ordered Assembly of the ESCRT-III Complex on Endosomes Is Required to Sequester Cargo during MVB Formation. Developmental Cell *15*, 578–589.

Teis, D., Saksena, S., and Emr, S.D. (2009). SnapShot: The ESCRT Machinery. Cell *137*, 182–182.e1.

Teis, D., Saksena, S., Judson, B.L., and Emr, S.D. (2010). ESCRT-II coordinates the assembly of ESCRT-III filaments for cargo sorting and multivesicular body vesicle formation. The EMBO Journal *29*, 871–883.

Wollert, T., and Hurley, J.H. (2010). Molecular mechanism of multivesicular body biogenesis by ESCRT complexes. Nature *464*, 864–869.

Xiao, J., Xia, H., Zhou, J., Azmi, I., Davies, B., Katzmann, D., and Xu, Z. (2008). Structural Basis of Vta1 Function in the Multivesicular Body Sorting Pathway. Developmental Cell *14*, 37–49.